ORIGINAL PAPER

Degradation of Plasticised Poly(lactide) Composites with Nanofibrillated Cellulose in Different Hydrothermal Environments

M. H. Wolf[1] · O. Gil-Castell[1] · J. Cea[2] · J. C. Carrasco[2] · A. Ribes-Greus[1]

Abstract

In this study, bionanocomposite films based on poly(lactide) (PLA) plasticised with poly(ethylene glycol) (PEG) (7.5 wt%) and reinforced with various contents of nanofibrillated cellulose (NFC) (1, 3, 5 wt%) were prepared. The hydrothermal degradation was investigated through immersion in several aqueous environments at temperatures of 8, 23, 58, and 70 °C as a function of time (7, 15, 30, 60, 90 days). The effect of water immersion on the physicochemical properties of the materials was assessed by monitoring the changes in the morphology, thermo-oxidative stability, thermal properties, and molar mass through field emission scanning electron microscopy (FE-SEM), thermogravimetric analysis (TGA), differential scanning calorimetry (DSC), and gel permeation chromatography (GPC). The hydrothermal degradation behaviour was not critically affected regardless of the nanofibrillated cellulose content. All the materials revealed certain integrity towards water immersion and hydrolysis effects at low temperatures (8 and 23 °C). The low hydrothermal degradation may be an advantage for using these PLA biocomposites in contact with water at ambient temperatures and limited exposure times. On the other hand, immersion in water at higher temperatures above the glass transition (58 and 70 °C), leads to a drastic deterioration of the properties of these PLA-based materials, in particular to the reduction of the molar mass and the disintegration into small pieces. This hydrothermal degradation behaviour can be considered a feasible option for the waste management of PLA/PEG/NFC bionanocomposites by deposition in hot aqueous environments.

Keywords Poly(lactide) (PLA) · Poly(ethylene glycol) (PEG) · Nanofibrillated cellulose (NFC) · Bionanocomposites · Hydrothermal degradation · Water immersion

Introduction

Biopolymers produced from renewable sources that are also biodegradable have gained much interest in the past decades due to rising oil prices and the problem of plastic waste management [1–3]. Poly(lactide) (PLA) is a promising biopolymer made from agricultural products such as corn, wheat or sugar beets and shows good mechanical properties, easy

processability and biodegradability [4]. Nevertheless, PLA has some drawbacks restraining large-scale industrial production, such as poor thermal resistance, inherent brittleness and low impact resistance [5]. A common way to improve impact resistance and crystallisation kinetics is to blend with other polymers that can act as plasticisers [6–8]. It has been reported that poly(ethylene glycol) (PEG) effectively improves the chain mobility, elongation at break, hydrophilicity, degradation rate, or softness of PLA [9–14]. In addition, PLA's properties can be tailored by adding fillers to the matrix, such as natural fibres [15–17]. Nanofibrillated cellulose (NFC) has been shown to significantly enhance PLA assets by promoting the crystallisation process, improving the mechanical properties, and modulating the water and air permeability [18–20]. Acetylation of NFC can improve the interphase between the PLA matrix and the fibres, to obtain a better and more uniform dispersion [9, 10]. At present PLA-based materials can be utilised in packaging [21–27], medicine [28–30], agriculture [31–33], electronics [34–36],

✉ O. Gil-Castell
ogilcastell@doctor.upv.es

✉ A. Ribes-Greus
aribes@ter.upv.es

[1] Instituto de Tecnología de Materiales (ITM), Universitat Politècnica de València (UPV), Camino de Vera, s/n, 46022 Valencia, Spain

[2] Unidad de Desarrollo Tecnológico (UDT), Universidad de Concepción, Avenida Cordillera, 3624, Parque Industrial Coronel, 4191996 Coronel, Chile

and automotive [37–39], where the behaviour in contact with water plays an important role. As a bio-polyester, PLA possesses labile bonds that can be hydrolytically broken by interaction with water molecules [40]. Gaining knowledge about the structural, thermal, and mechanical changes undergone through hydrothermal degradation is crucial for extending the application range and managing the waste of PLA-based bionanocomposites.

PLA has been reported as relatively stable in water at temperatures below the glass transition, while higher degradation rates occur above the glass transition [41, 42]. Water molecules can penetrate into the polymer structure and act as a plasticising agent by increasing the mobility of molecules, and promoting relevant physico-chemical changes [43]. Furthermore, adding hydrophilic components, such as PEG and NFC, can make the materials more attractive to water and impact their hydrothermal stability in contact with aqueous solutions [44, 45].

Although the water absorption behaviour of PLA-based materials containing PEG is well documented, changes in the performance of plasticised bionanocomposites reinforced with NFC promoted by hydrothermal degradation, especially at different temperatures, still needs to be investigated [32, 46–48]. For this purpose, a simulation of hydrothermal ageing is an excellent tool to ascertain the degradation behaviour of biocomposites during their hypothetic service life exposed to various humid environments [41, 49]. Therefore, this work aims to implement a detailed investigation of the hydrothermal degradation behaviour of bionanocomposite films based on poly(lactide) (PLA) with poly(ethylene glycol) (PEG) as a plasticiser (7.5 wt%) and nanofibrillated cellulose (NFC) as a reinforcement filler (1, 3 and 5 wt%) in different simulated environments. The temperatures of 8, 23, 58, and 70 °C selected for the water immersion provide a broad overview of the hydrothermal degradation process that simulates various applications and end-of-life scenarios, and are all of them motivated in Table 1.

The consequences of exposure to hydrothermal degradation conditions in these humid environments were assessed based on the mass variation, visual appearance, surface morphology, thermo-oxidative stability, crystalline structure, and molar mass as a function of immersion time. These parameters were monitored during different extractions after 7, 15, 30, 60, and 90 days.

Materials and Methods

Materials and Reagents

Poly(lactide) (PLA) pellets (Grade 4032D) were supplied by Nature Works LLC (Minnetonka, USA) with a D-isomer content of 1.6%. According to the manufacturer, the grade 4032D is well suited for thermoforming, coating, injection moulding, blow moulding, and fibre applications. Poly(ethylene glycol) (PEG) with a molar mass of 1500 g mol^{-1} from Merck (Darmstadt, Germany) was added as a plasticising agent. Nanofibrillated cellulose (NFC) was obtained from Eucalyptus Bleached Kraft Pulp (80% *Eucalyptus globulus* and 20% *Eucalyptus nitens*) in form of sheets, supplied by CMPC Pulp S.A. Santa Fe Mill (Nacimiento, Chile). Tetrahydrofuran (THF) ($\geq 99.8\%$) used as a mobile phase in gel permeation chromatography was supplied by Scharlau (Barcelona, Spain).

Table 1 Temperatures selected for the water immersion studies

Temperature	Motivation
8 °C	• Occurs during the storage of e.g. food packaging in a refrigerator • Simulates natural environments, such as rivers and lakes, and shows the degradation of PLA/PEG/NFC composites if waste enters these cold, humid places

23 °C	• Represents standard room temperature, which is dominantly used for storing packaging materials
	• It is also the typical temperature used in the standards:
	  ◦ EN-ISO 62 "Plastics—Determination of water absorption" [50]
	  ◦ ASTM D570-98 "Standard Test Method for Water Absorption of Plastics" [51]

58 °C	• It is used for biodegradation studies [52, 53], for example, in the following standards:
	  ◦ ASTM D6400-04 "Standard Specification for Compostable Plastics" [54]
	  ◦ ASTM D5338-11 "Standard Test Method for Determining Aerobic Biodegradation of Plastic Materials under Controlled Composting Conditions" [55]
	  ◦ DIN EN 13432:2000-12 "Packaging Requirements for Packaging Recoverable through Composting and Biodegradation Test Scheme and Evaluation Criteria for the Final Acceptance of Packaging" [56]
	  ◦ ISO 14855-2 "Determination of the Ultimate Aerobic Biodegradability of plastic materials under Controlled Composting Conditions" [57]

70 °C	• Simulates applications in automobile or electronic parts where higher temperatures can occur • Allows seeing the hydrothermal degradation behaviour over the glass transition of PLA ($T_g = \sim 55$ °C) in the rubbery state of the materials

Preparation of Nanofibrillated Cellulose (NFC)

Kraft pulp sheets were processed by grinding until disintegrated fibres with a size of less than 1 cm were obtained. The fibres were then partially acetylated with glacial acetic acid (180 °C, 2 h, solid/liquid ratio 1/20) and recirculated in a laboratory disc refiner operating at 2500 rpm for 40 passes to ensure size reduction and homogeneity of the NFCs. Subsequently, after cooling, the NFC suspension was diluted in heptanol and heated to remove the acetic acid, which has a lower boiling point. Finally, water was added to displace the heptanol from the NFC and to separate it by decantation, so that the fibres were not dried during these processes and hornification was avoided.

The prepared acetylated NFC have a degree of substitution of 0.52, determined by titration according to Rodrigues Filho et al. [58], and an average diameter of 30 nm, determined by the intrinsic viscosity according to the model of Albornoz-Palma et al. [59] (parameters: $[\eta] = 1003$ mL g^{-1}, average length = 8.1 μm). The morphology of the NFC can be appreciated in the scanning electron micrograph shown in Fig. S1 in the Supplementary Information.

Preparation of PLA/PEG/NFC bionanocomposites

For the composite preparation, the PLA pellets were preliminarily dried at 80 °C for 2 h to remove the moisture. Then, PEG was combined with the NFC suspension in a DLAB MS-H280-PRO magnetic hot plate (Beijing, China) at 120 °C for 40 min to achieve a homogeneous dispersion. Next, prior to compounding with PLA, the PEG/NFC mixtures were placed in an oven at 100 °C for 2 h to remove the humidity. Afterwards, the mixtures and the PLA pellets were combined in a Brabender 815653 torque rheometer (Duisburg, Germany) at 180 °C for 5 min and 50 rpm. The partial acetylation of NFC allows the improvement of the interface between the PLA matrix and fibres, obtaining a more uniform dispersion [60, 61].

For the PLA/PEG blend, 7.5 wt% plasticiser was added, and for the composites, NFC proportions of 1, 3, and 5 wt% were included, based on the sum of the mass of PLA and PEG. Therefore, actual proportions of the all the components in the resulting materials were calculated, as shown in Table 2. For the sake of clarity, bionanocomposite compositions were labelled according to the entire numeral of NFC weight percentage.

The different compositions were injection moulded into Type IV ASTM D638 dog-bone specimens and further processed through thermo-compression to obtain the film specimens [62]. A HAAKE MiniJet II setup (Vreden, Germany) was used for the injection, with a preheating stage at 190 °C for 2 min. The temperature of the moulds was 55 °C, and the injection and post-pressure were 400 bar and

Table 2 Designation and composition of the PLA, PLA/PEG and PLA/PEG/NFC materials

Designation	PLA (wt%)	PEG (wt%)	NFC (wt%)
PLA	100.00	–	–
PLA/PEG	92.50	7.50	–
PLA/PEG/NFC1	91.59	7.42	0.99
PLA/PEG/NFC3	89.81	7.28	2.91
PLA/PEG/NFC5	88.10	7.14	4.76

300 bar, respectively. Subsequently, flat rectangle sheets were obtained through compression moulding using a custom-made four-axis hot plate press. First, each material got preheated at 190 °C for 10 min. Afterwards, the material got pressed into a PTFE mould with a pressure of 50 kg cm^{-2} for 3 min, followed by a pressure of 75 kg cm^{-2} for 3 min and 100 kg cm^{-2} for another 3 min. After compression, the samples were removed from the hot press and cooled at room temperature. The obtained sheets were cut into smaller stripes with the dimensions of 3.0×1.0 cm^2 and a thickness of 0.5 ± 0.1 mm. The thickness was measured with a Comparator Stand (type BS-10 M) from Mitutoyo at five different locations, and the average was calculated and used respectively for future calculations. Afterwards, the specimens were placed in zip bags and stored in a desiccator at room temperature until further analysis [63].

Water Immersion

The water immersion was monitored in terms of gravimetric change, as adopted from the standard EN-ISO 62:2008 "Plastics—Determination of water absorption" [50]. The water temperatures were 8, 23, 58 and 70 °C, as motivated in Table 1.

For the water absorption studies, the samples were firstly dried in a vacuum oven Heraeus Vacutherm VT 6025 (Langenselbold, Germany) at 30 °C for 24 h to remove the remnant moisture. Subsequently, the mass of the dried samples (m_0) was determined with a Mettler Toledo AB135-S scale (Columbus, OH, USA). Then, the samples were placed in glass vials with a volume of 19 mL filled with distilled water and threaded with PTFE plugs to ensure the conditions of complete contact of the exposed surface with water. The temperatures of 23, 58, and 70 °C were carried out in different ovens from Heraeus Instruments Type B 12 (Hanau, Germany). The environment of 8 °C was carried out in a fridge from Aspes Type 4FAC4858 (Mondragón, Spain). After specific periods of immersion, the samples were taken out of the water to determine the mass (m_t). Before weighing, all traces of water on the surface were removed with a clean paper tissue. The mass as a function of time (M_t),

with which mass variation profiles were constructed, was calculated according to Eq. (1).

$$M_t(\%) = \frac{(m_t - m_0)}{m_0} \cdot 100 \tag{1}$$

Material Characterisation Techniques

Field-Emission Scanning Electron Microscopy (FE-SEM)

The surface morphology was examined with a Zeiss Ultra 55 field-emission scanning electron microscope (Oberkochen, Germany). The specimens were cut into small pieces and mounted on metal studs. They were sputter-coated with platinum for 15 s using a Leica EM MED020 high-resolution sputter coater (Wetzlar, Germany). While testing, a voltage of 1.50 kV, with a working distance of around 5 mm and a temperature of 22 °C were considered. The pictures taken for the samples have a magnification of 5000×.

Thermo-gravimetric Analysis (TGA)

The thermo-oxidative stability was determined with the Mettler-Toledo TGA 851 equipment (Columbus, OH, USA). A heating circulator type F32-HL from Julabo GmbH (Seelbach, Germany) was used for thermal control. The samples with a mass of about 4 mg were placed into 40 mL alumina crucibles from Mettler-Toledo. A dynamic thermo-gravimetric procedure with a heating rate of 10 °C min^{-1} in the temperature range of 25–800 °C was considered. An oxidative atmosphere with oxygen (O_2) as the gas with a flow rate of 50 mL min^{-1} was used. Two specimens for each sample were analysed. TGA analyses were performed with the software STARe (version 9.01) from Mettler-Toledo. To evaluate the thermal stability of the materials, the peak temperature (T_{peak}) of the derivative thermogravimetric curve (DTG), as well as the extrapolated onset temperature of the sigmoidal thermogravimetric curve (T_{onset}), where the horizontal baseline crosses the tangent of inflection point, were determined following the ISO 11358–1 standard [64]. The averages of the values from each sample were taken respectively.

Differential Scanning Calorimetry (DSC)

Calorimetric data were determined with the Mettler-Toledo DSC 820 setup (Columbus, OH, USA) coupled with a cooling system type Haake EK 90/MT from Thermo Fisher Scientific (Waltham, USA). The samples with a mass of about 4 mg were placed into 40 mL aluminium crucibles from Mettler-Toledo perforated on top to allow gas evaporation. The temperature range between 0 and 200 °C was run with a heating/cooling rate of 10 °C min^{-1}. All measurements used

nitrogen (N_2) with a flow rate of 50 mL min^{-1} as a protective gas to prevent oxidative reactions of the samples. The scanning program consisted of three subsequent heating/cooling/heating segments with 3-min-long isotherms for stabilisation. Two samples for each specimen were measured, and the obtained values were averaged. The DSC analyses were performed with Mettler-Toledo's software STARe (version 9.01).

Different values were gathered from the DSC measurements to gain information about the various phase transitions and the crystallinity of the composites. The values of the first heating scan were taken respectively for further calculations because it allows the determination of the present sample condition after the preparation through compression moulding, immersion in water, and storage. From the first heating scan, the enthalpy of the cold crystallisation process (Δh_{CC}) and the melting process (Δh_M) were gained through the integration of the DSC-curve. The degree of crystallinity (X_c) of the materials was calculated with the obtained values using Eq. (2).

$$X_c(\%) = \frac{\Delta h_M - \Delta h_{CC}}{w \cdot \Delta h_{M0}} \cdot 100 \tag{2}$$

where Δh_M and Δh_{M0} are the melting enthalpies for the PLA samples and 100% crystalline PLA, Δh_{CC} is the enthalpy of the crystallisation event, and w is the weight fraction of PLA in the composite. A value of 93 J g^{-1} was taken as the melting enthalpy of a totally crystalline PLA material (Δh_{M0}) [65].

Furthermore, it is possible to evaluate the crystalline structure by calculating the lamellar thickness (l_c) with the Thomson-Gibbs equation [66], represented in Eq. (3).

$$l_c(T_M) = \left[\left(1 - \frac{T_M}{T_M^0} \right) \cdot \frac{\Delta h_{MV}}{2 \cdot \sigma_e} \right]^{-1} \tag{3}$$

where T_M is the obtained peak temperature of the melting procedure, T_M^0 is the equilibrium melting temperature of an infinite crystal (480 K), σ_e is the surface free energy of the basal plane where the chains fold (60.89·10^{-3} J m^{-2}), and Δh_{MV} is the melting enthalpy per volume unit (111.083·10^6 J m^{-3}) [67].

Gel Permeation Chromatography (GPC)

The molar mass was evaluated with an Omnisec gel permeation chromatography (GPC) system from Malvern Panalytical (Worcestershire, United Kingdom). The system consists of the Resolve section with an integrated pump, a degasser, an autosampler and a column oven, and the Reveal part with a multi-detector including Ultraviolet, Refractive Index, Low- and Right-Angle Scattering and Viscosity.

The measuring system was calibrated before and after each sequence using a monodisperse polystyrene (PS) standard (105 000 g mol^{-1}). Two columns from Malvern Panalytical were used (T2000 and T4000, both 300 mm $\times$ 8 mm) at a temperature of 35 °C. Tetrahydrofuran (THF) was used as a mobile phase with a flow rate of 1.0 mL min^{-1}. The samples were dissolved in THF with a concentration of ca. 2.0 mg mL^{-1} at 58 °C for 48 h and filtered through 0.45 μm PTFE filters. Two injections of 100 μL per sample were performed, and the obtained data were analysed with the Omnisec V11™ software. As a result, the molar mass distribution was obtained, along with other parameters, such as the number average molar mass (M_n) and the weight average molar mass (M_w).

Results and Discussion

In this study, the effects of water immersion on the gravimetric mass, visual appearance, surface morphology, thermo-oxidative stability, crystalline structure, and molar mass of the PLA, plasticised PLA/PEG, and PLA/PEG/NFC bionanocomposites are presented and compared to the non-immersed materials. Afterwards, given the simultaneous influence of hydrothermal degradation by multiple factors, such as the immersion time (0, 7, 15, 30, 60, and 90 days), immersion temperature (8, 23, 58, and 70 °C), and the composition of the materials, a statistical approach was applied

to quantify their isolated effects. As for the composition, the contribution of poly(ethylene glycol) (PEG) as a plasticiser alongside nanofibrillated cellulose (NFC) as a reinforcement filler was analysed and compared to pure poly(lactide) (PLA). The possibilities and limitations of using these PLA-based bionanocomposites in the simulated wet environments of typical bioplastic applications were consequently displayed and examined.

Monitoring of Mass and pH Variation During Immersion

The mass variation curves at different immersion temperatures (8, 23, 58, and 70 °C) are shown in Fig. 1. Mass changes were monitored for a maximum period of 90 days at 8 and 23 °C, while at 58 and 70 °C they had to be stopped after ~ 30 days and ~ 10 days, respectively, because the samples started to get vastly disintegrated, making them impossible to be measured.

Pure poly(lactide) (PLA) absorbs water during immersion at all temperatures and achieves a steady equilibrium. In contrast, the samples containing poly(ethylene glycol) (PEG) lose mass after reaching a maximum of water absorption, resulting in a peak-like curve progression, as can be appreciated in the inset of Fig. 1 for the early stages of immersion at the temperature of 23 ºC. This phenomenon has been ascribed to the release of species such as short polymer segments, additives, plasticisers, or fillers, which can begin to

Fig. 1 Mass variations of the PLA, PLA/PEG and PLA/PEG/NFC films through immersion in water at different temperatures (8, 23, 58, and 70 °C)
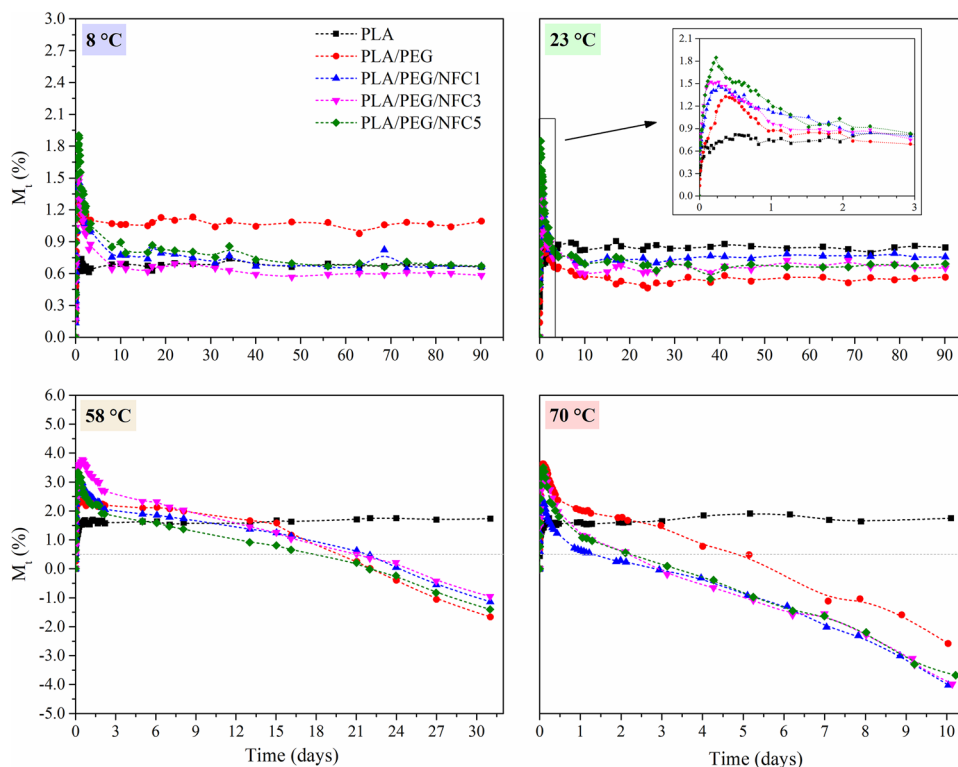
leach and dissolve due to their poor interaction and freedom of movement [68–71]. After the peak, the curves of the PLA/PEG blend and the PLA/PEG/NFC bionanocomposites for the immersion temperatures of 8 and 23 °C remain constant, while those for 58 and 70 °C continue to decline linearly until disintegration. The plasticised samples immersed in water at 58 °C progressively lose ca. 5.0% of mass after 30 days, while the specimens immersed at 70 °C lose ca. 7.5% after 10 days. This constant mass loss at higher temperatures is supposed to be due to the release of hydrolysed soluble oligomers that can escape from the matrix [72].

At this point, to further investigate the hydrothermal performance, the pH of the aqueous solutions was measured as a function of time, as presented in Fig. 2. At 8 °C, the pH of the solutions for pure PLA and the PLA/PEG blend remains unaltered, while that of the PLA/PEG/NFC bionanocomposites decreases from the very first stages of water immersion, more significantly as the NFC percentage increased. This behaviour suggests that the PLA/PEG/NFC bionanocomposites had more low molar mass acidic compounds than pure and plasticised PLA, that were released during immersion. These compounds with low molar mass could have been created during processing in the torque rheometer, when PEG and NFC were added to the PLA. Other authors showed that adding fillers during melt processing can alter the rheological behaviour of the melt as a consequence of the filler-matrix interface and the presence of short-range interactions via overlapping of interfacial layers on neighbouring fillers [73]. This effect may produce higher shear forces during processing and enhance thermo-mechanically induced chain scission. This influence, together with the hydrophilic nature of NFC, which can lead to the absorption of small amounts of water and hydrolytic chain scission during processing [74], can lead to greater degradation. A similar but more accentuated pH decrease was visible during immersion at 23 °C, also showing a reduction for the pure PLA and PLA/PEG films. Here, temperature contribution gained importance, revealing a more significant acidic compound's release. At 58 °C, an even stronger pH loss was found with a slower decreasing behaviour for PLA compared to plasticised PLA and bionanocomposites. Finally, at 70 °C, a sharp pH decrease for all the materials was observed after only 15 days.

These observations suggest that 8 °C did not provide enough thermal energy to promote a significant mass loss due to hydrolytic breakage during immersion but highlight the contribution of NFC during processing, which could have generated low molar mass compounds with carboxyl end groups that were released from the first stages of immersion and decrease the pH. At 23 °C, the reduction of pH for all the compositions, more accentuated with the presence of NFC, demonstrates that all the materials underwent hydrolytic degradation during immersion. Additionally, water immersion at higher temperatures of 58 and 70 °C above the glass transition of PLA promoted an extensive hydrolytic scission of ester bonds and subsequent leaching of acidic

Fig. 2 pH variations of the solutions during immersion in water of PLA, PLA/PEG and PLA/PEG/NFC films at different temperatures (8, 23, 58, and 70 °C)
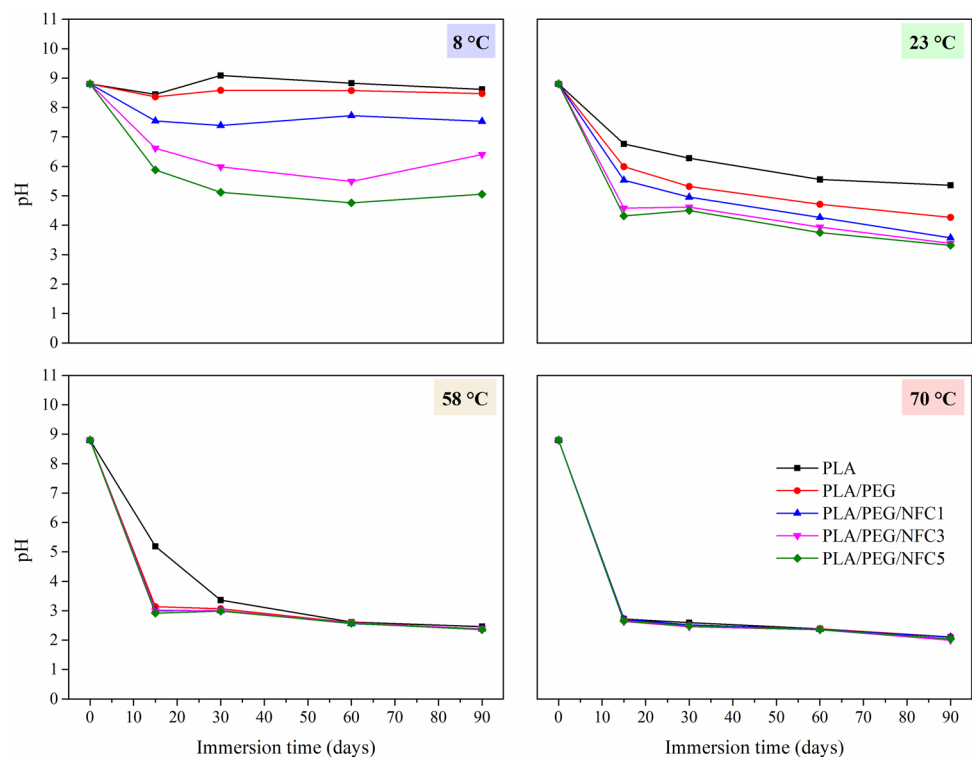
compounds [75], which strongly influenced the mass of the films and the pH of the remnant solutions.

Macroscopic Changes

The macroscopic changes during immersion were monitored, and the visual appearance of the films is shown in Table 3. Raw PLA remains transparent after immersion at 8 and 23 °C, while the PLA/PEG blend and the PLA/PEG/NFC bionanocomposites develop small white dots, which become more prominent with time. Additionally, the PLA/PEG blend and PLA/PEG/NFC bionanocomposites immersed at 23 °C slowly lose their transparency and become whitish as a function of time.

At 58 °C, the materials became opaque and showed multiple white spots after only 15 days. After 30 days, the films were completely white with a very fragile behaviour. At longer immersion times, these samples develop cracks, collapse and disintegrate into small parts. The visual changes of the samples stored in water at 70 °C occur even faster and more drastically. Indeed, after 90 days of immersion at 70 °C, the materials disintegrated so far that it was impossible to manage them properly.

Overall, at lower temperatures of 8 and 23 ℃, the polymer chains maintain the morphology and structure determined by processing below the glass transition. In comparison, the immersion at higher temperatures of 58 and 70 °C favours water penetration and more kinetic energy that may act as driving forces for increased chain mobility and hydrolytic cleavage, which provoked significant changes in the visual appearance likewise found in other studies immersing PLA-based composites [76]. Most of these changes have been associated with a preferential degradation of amorphous regions and increased material crystallinity [68, 77, 78], significantly increasing opacity [79].

Microscopic Surface Morphology

The surface morphology of the samples at a microscopic level before and after 60 days of water immersion is presented in Table 4. In addition, the electron micrographs of the samples after 30 days of immersion can be found in the Supplementary Information in Table S1.

After the immersion in water at 8 and 23 °C for 60 days, the film specimens remained practically stable and showed a characteristic plane surface with small stripes caused by compression moulding during sample preparation. In contrast, above the glass transition temperature at 58 ℃, the PLA, the PLA/PEG blend and the PLA/PEG/NFC bionanocomposites show clear pores and cracks on the surface of films. The cracks and pores of the materials get more extensive, resulting in a further rough and uneven surface as degradation progresses. More drastic morphological changes

occur at the highest water immersion temperature of 70 °C, resulting in a sponge-like porous structure. Equally looking pores were found by Fukushima et al. due to the immersion of PLA at elevated temperatures [76]. This structure is suggested to occur because parts of the amorphous regions may have been hydrolysed during immersion and disappeared, leaving the crystalline structures behind [80, 81]. This performance is coherent with the perceived mass loss and pH reduction due to the release of acidic substances from the bionanocomposite.

Particularly, at 58 and 70 ℃, the PLA/PEG blend and the PLA/PEG/NFC bionanocomposites show dominant cracks on the face of the films, more restrained with increasing nanofibrillated cellulose (NFC) content. The presence of NFC seems to enhance the integrity of the PLA/PEG-based films, contrarily to what has been reported for PLA-based biocomposites with hydrophilic micro or macro-fillers, where they act as water attracting elements with differential swelling to matrix, developing stress at interphase region leading to microcracking [41, 68]. Even though PLA/PEG blends are highly hydrophilic, the inclusion of low percentages of NFC with functional groups in his surface, can interact with PLA and PEG domain and act as a cohesive agent [82], therefore contributed to reduce the cracking phenomena during immersion.

Thermo-oxidative Stability

The obtained derivative thermogravimetric (DTG) thermograms of the immersed PLA, PLA/PEG and PLA/PEG/NFC samples at 8, 23, 58 and 70 °C are shown in Fig. 3, involving a main mass loss stage at 350 ℃ with a mass loss of ca. 95%, typical for PLA-based materials. Complementarily, the thermograms of PLA/PEG and PLA/PEG/NFC revealed the decomposition peak of PEG at around 250 °C. As mentioned before, after 90 days of immersion in water at 70 °C, the samples got vastly disintegrated, and consequently, TGA analysis could not be performed. The immersion in water at 8 and 23 °C seem to have no significant effect on the thermo-oxidative stability, regardless of the composition, as indicated by the overlapping of the obtained thermograms for all immersion times. On the other hand, the immersion at 58 and 70 °C clearly shifts the decomposition step of the materials towards lower temperatures as a function of immersion time, especially in terms of the onset temperature. The corresponding TG thermograms, which can be found in the Supplementary Information in Fig. S2, corroborate the shift towards lower temperatures of the onset of the decomposition process, that takes place over a wider temperature range, also with a more heterogeneous behaviour as a function of immersion time. Although it was non-critical, the effect of NFC could be appreciated at long immersion times particularly at 58 ℃, contributing to retain
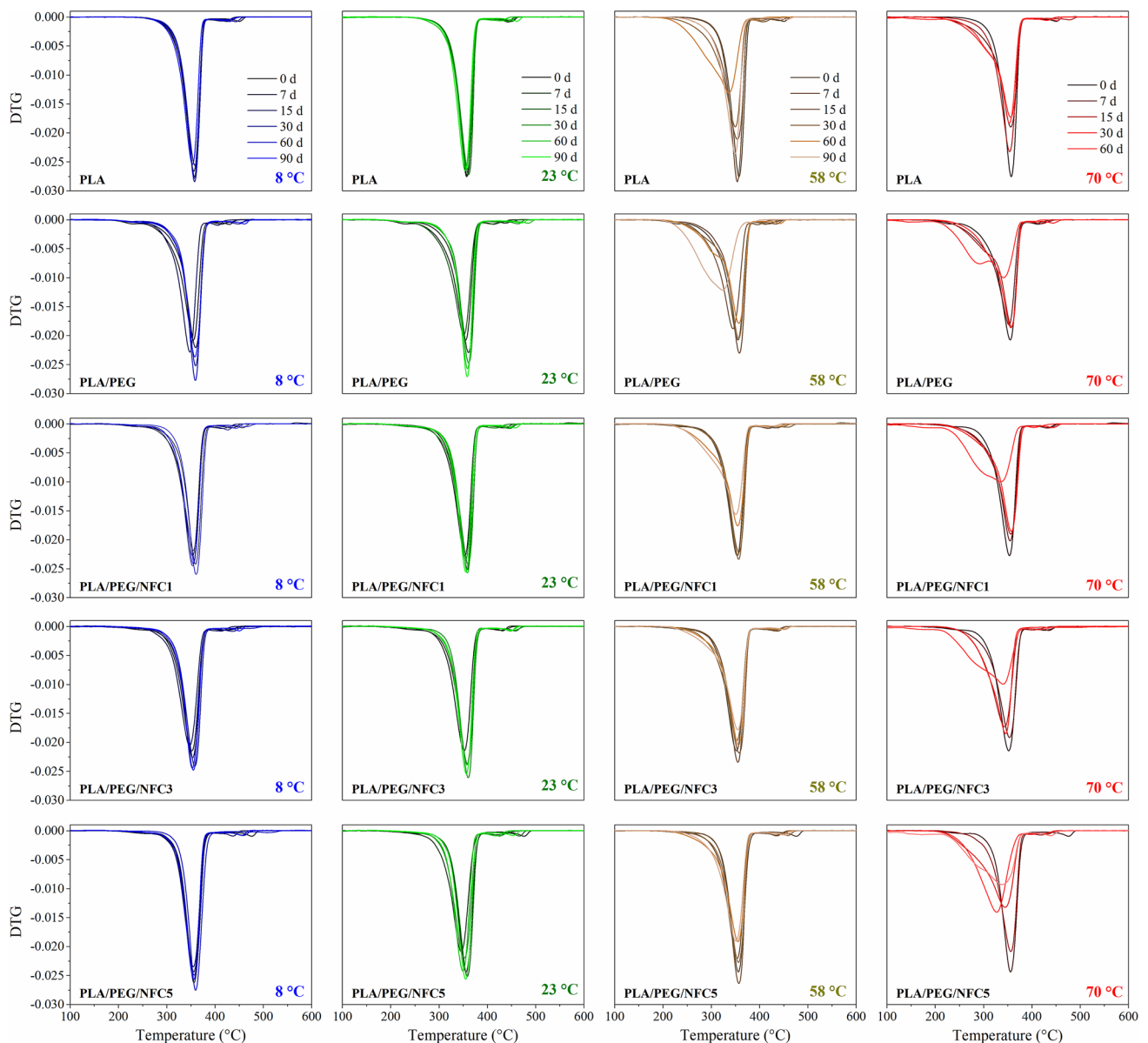
Fig. 3 DTG thermograms of the PLA, PLA/PEG and PLA/PEG/NFC films before and after the immersion in water at different temperatures (8, 23, 58, and 70 °C) for different times (0, 7, 15, 30, 60, and 90 days)

to a greater extent the characteristic shape and temperatures of the thermo-oxidative decomposition process of the non-immersed samples. The cohesive effect of NFC intuited in previous section may have contributed to reduce the oxygen penetration pathways during thermogravimetric analyses and, therefore, retain certain thermo-oxidative stability.

Thermal Phase Transitions and Crystalline Structure

The hydrothermal degradation kinetics of PLA are known to be affected by the initial crystallinity and can also promote changes in its crystalline structure during immersion

[83]. In fact, the hydrolysis reaction is influenced by the water diffusion into the amorphous parts, which are more labile to degradation and can undergo rearrangements into crystalline domains [78], in agreement with previous microscopic results.
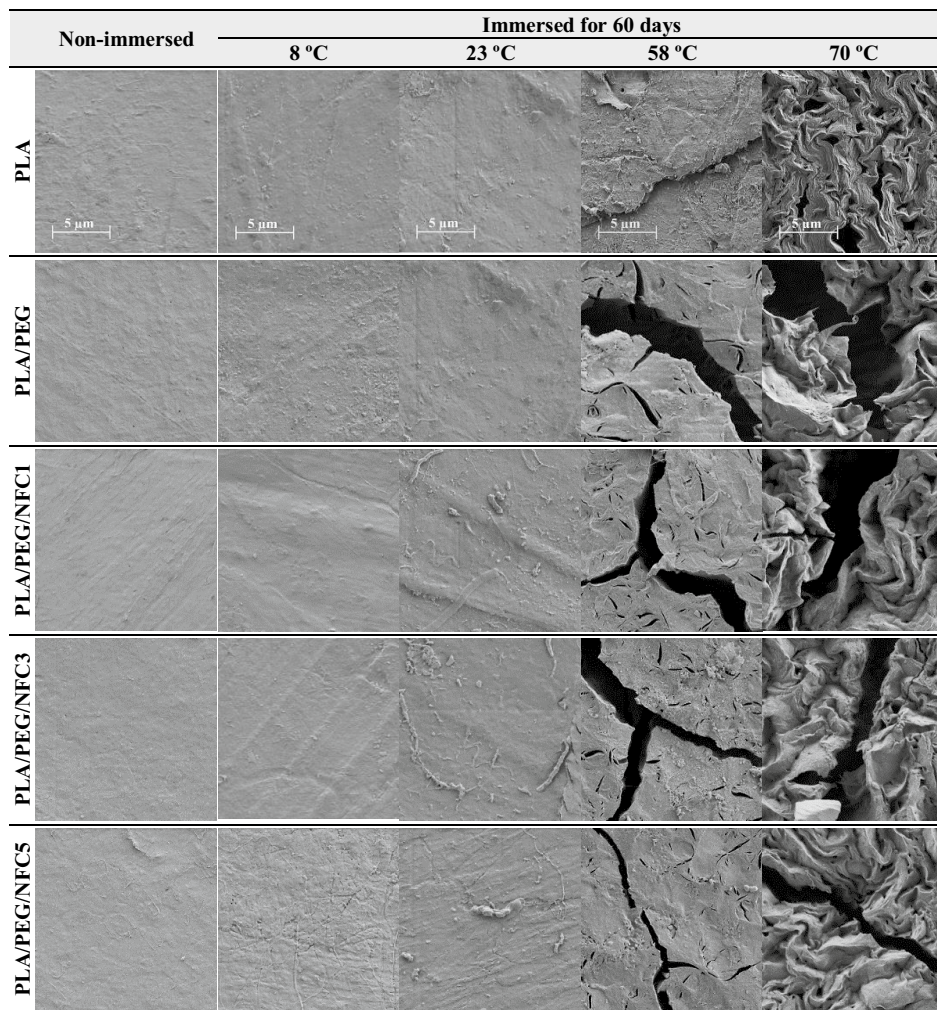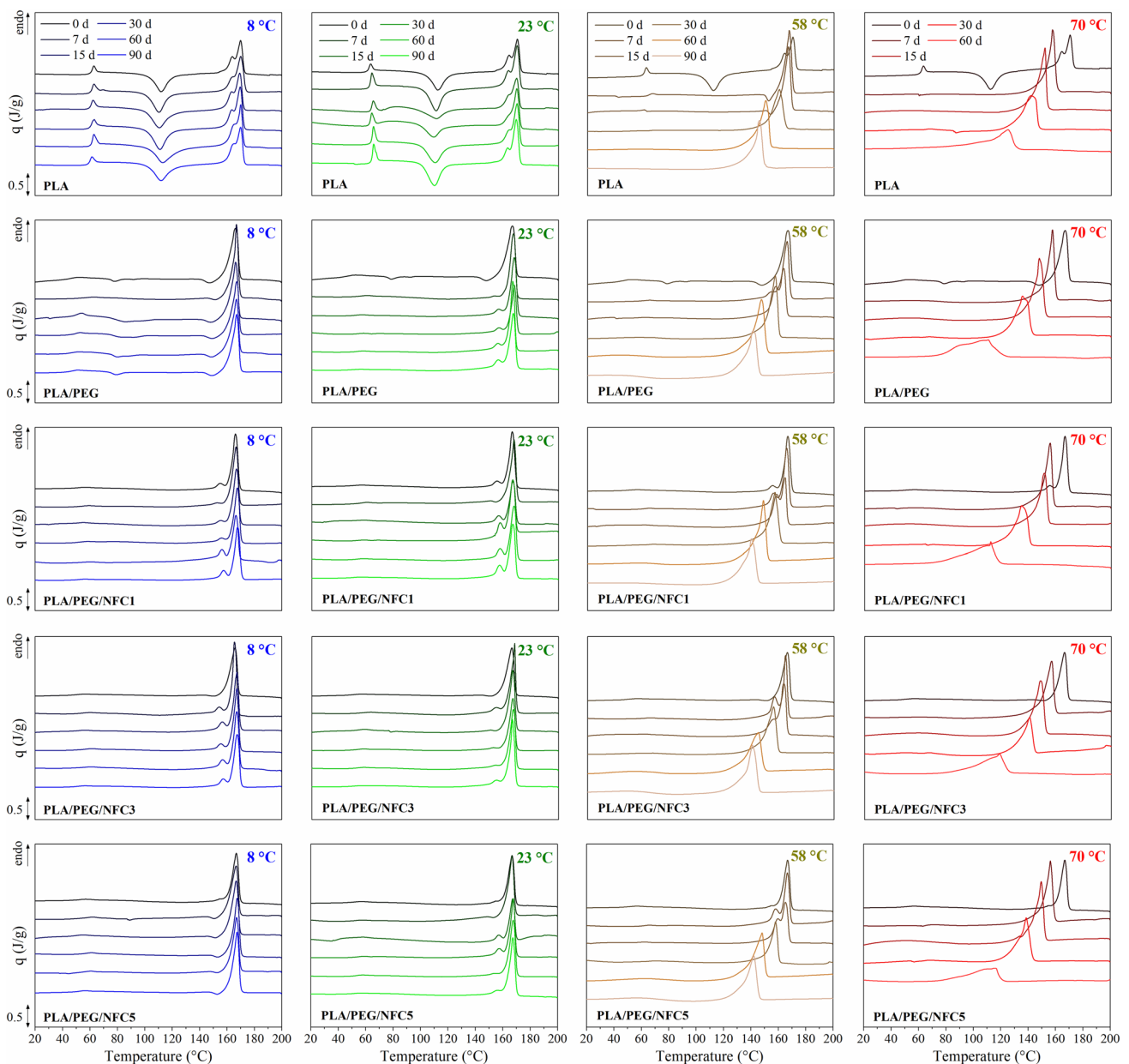
The calorimetric thermograms for the first heating scan were chosen for the evaluation because they represent the present thermal properties of the materials after immersion and can be seen in Fig. 4 for the different compositions, immersion temperatures and times. The thermograms for the cooling and the second heating scans can be found in Fig. S3 and Fig. S4 in the Supplementary Information.

Table 3 PLA, PLA/PEG and PLA/PEG/NFC films after immersion in water at different temperatures (8, 23, 58, 70 °C) and times (0, 15, 30, 90 days)

	8 °C					23 °C				
	0 days	15 days	30 days	60 days	90 days	0 days	15 days	30 days	60 days	90 days
PLA										
PEG[a]										
NFC1[b]										
NFC3[c]										
NFC5[d]										
	58 °C					70 °C				
	0 days	15 days	30 days	60 days	90 days	0 days	15 days	30 days	60 days	90 days
PLA										
PEG[a]										
NFC1[b]										-
NFC3[c]										
NFC5[d]										
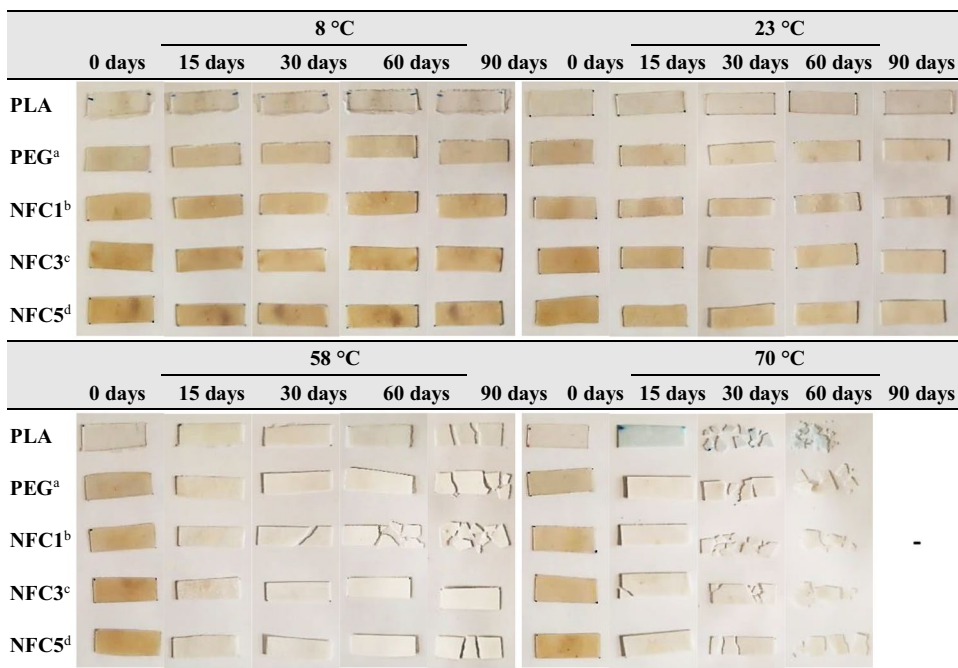
[a]PLA/PEG, [b]PLA/PEG/NFC1, [c]PLA/PEG/NFC3, [d]PLA/PEG/NFC5

Table 4 Micrographs of the PLA, PLA/PEG and PLA/PEG/NFC films before and after the immersion in water at 8, 23, 58 and 70 °C for 60 days

	Non-immersed	Immersed for 60 days			
		8 °C	23 °C	58 °C	70 °C
PLA					
PLA/PEG					
PLA/PEG/NFC1					
PLA/PEG/NFC3					
PLA/PEG/NFC5					

Fig. 4 DSC thermograms of the first heating scan of the PLA, PLA/PEG and PLA/PEG/NFC films before and after the immersion in water at different temperatures (8, 23, 58, and 70 °C) for different times (0, 7, 15, 30, 60, and 90 days)

Before water immersion, raw PLA exhibits a glass transition with a structural relaxation followed by a cold crystallisation and a melting process consisting of two overlapping peaks ascribed to two dissimilar crystalline populations. The PLA/PEG blend and the PLA/PEG/NFC bionanocomposites show less significant structural relaxations, smaller cold crystallisations, and a more prominent unimodal melting peak.

From the thermograms of the samples stored in water at 8 and 23 °C, phase transitions remained virtually stable.

However, the immersion at the higher temperatures of 58 and 70 °C caused both the structural relaxation and cold crystallisation to vanish. Analogous results for PLA during accelerated ageing have been reported [42, 79, 84]. This phenomenon is supposed to occur due to an increased crystallinity during water immersion that might prevent the rearrangement of the polymer chains when subjected to the heating program in the DSC. In addition, the melting peak generally shifted towards lower temperatures and became broader and smaller as a function of immersion time, especially visible

at 70 °C. Particularly for the PLA/PEG blend and the PLA/PEG/NFC bionanocomposites, the melting transition develops from a regular peak into an asymmetric shape, which was also found by other studies for PLA-based materials [68, 85–87]. Nijenhuis et al. and Yasuniwa et al. attributed this behaviour to lamellar rearrangements during the crystallisation of PLA, resulting in a second low-temperature peak of a new crystalline population on top of the original crystallites [86, 88].

Hydrothermal Chain Scission

The molar mass distributions of raw PLA, the PLA/PEG blend, and the PLA/PEG/NFC bionanocomposites after different immersion times in water at different temperatures are shown in Fig. 5.

For the samples immersed at 8 °C, non-significant alteration of the molar mass distributions was noticed, while at 23 °C, they slightly shifted to lower molar mass values. In contrast, the distributions of raw PLA, the PLA/PEG blend, and the PLA/PEG/NFC bionanocomposites
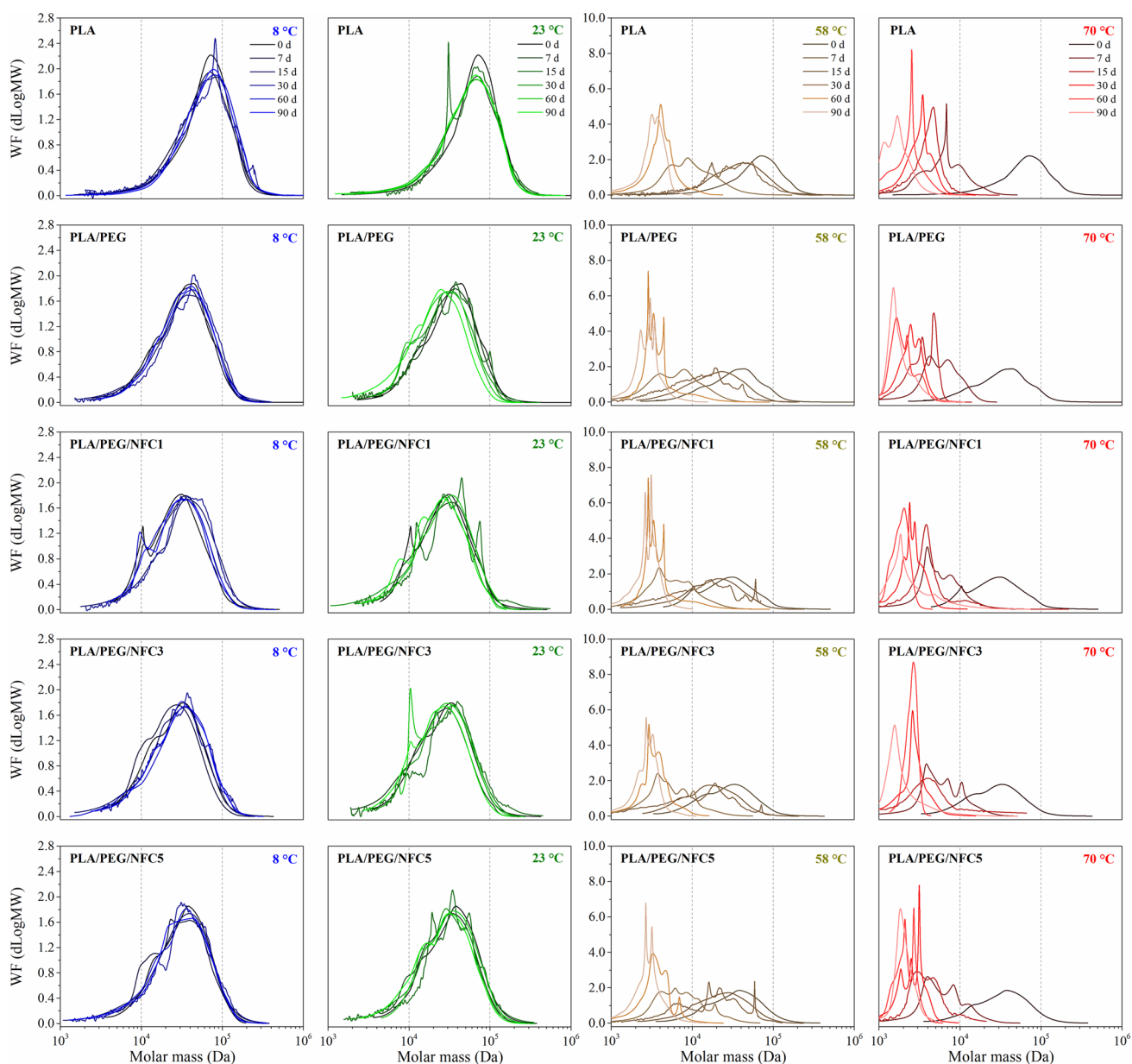
Fig. 5 Molar mass distributions of the immersed PLA, PLA/PEG and PLA/PEG/NFC films at 8 °C, 23 °C, 58 °C, and 70 °C (from top to bottom) after different immersion times (0, 7, 15, 30, 60, and 90 days)

immersed at 58 and 70 °C show a clear displacement towards lower values and a more heterogeneous profile as a function of time regardless of the composition, demonstrating a strong decrease in molar mass. The change in the shape of the distributions is a consequence of chain breakage and possible rearrangement or functionalisation of the polymer segments. Generally, hydrothermal degradation of PLA-based materials is a vastly heterogeneous process that can lead to non-gaussian performance [71]. Water immersion causes cleavage of the ester bonds, which leads to shorter polymer segments with smaller molar masses. The breakdown of the polymer structure into smaller segments is random and can result in the appearance of many different peaks in the distributions. Moreover, some authors suggest that the degradation products are formed both at the surface, and in bulk, and in the amorphous and crystalline regions with different degradation rates [71]. These results are consistent with the heterogeneous weight loss profiles due to hydrothermal degradation observed by the thermogravimetric measurements and with the changes in the acidity of the remnant aqueous solutions in the previous sections.

Influence of Immersion Time, Temperature, and Material Composition on Hydrothermal Degradation

In this study, the hydrothermal degradation is simultaneously influenced by multiple factors, such as the immersion time, immersion temperature, and the composition of the materials. Complementarily to the detailed results shown in previous sections, an overall perspective given by a statistical approach was made to quantify the effects of these factors. Therefore, the values for some of the assessed indicators of the physico-chemical characteristics of the bionanocomposites were selected: the onset temperature (T_{onset}) and the peak temperature (T_{peak}) of the main thermo-oxidative decomposition step, the degree of crystallinity (X_c) and lamellar thickness (l_c), as well as the average molar mass in number (M_n) and the average molar mass in weight (M_w). The values of these indicators are plotted in the Supplementary Information in Fig. S5, Fig. S6, and Fig. S7.

In order to have an isolated look at the influencing factors, the chosen numeric values were added together for the respective levels, and the arithmetic means were calculated and gathered in Table 5. Through this procedure, the influence of a single factor can be studied, while the

Table 5 Arithmetic means of the onset-temperature (T_{onset}-mean) and peak-temperature (T_{peak}-mean) of the main decomposition step, the degree of crystallinity (X_c-mean) and lamellar thickness (l_c-mean), and the average molar mass in number (M_n-mean) and average molar mass in weight (M_w-mean) for the various factors (immersion time, immersion temperature, material composition before and after water immersion) and their respective levels

Factor	Level	T_{onset}-mean (°C)	T_{peak}-mean (°C)	X_c-mean (%)	l_c-mean (nm)	M_n-mean (kDa)	M_w-mean (kDa)
Immersion time	0 d	329.1 (±2.4)	355.7 (±2.1)	37.0 (±1.8)	13.2 (±0.0)	26.6 (±0.7)	45.4 (±0.7)
	7 d	328.1 (±3.4)	355.6 (±2.3)	48.5 (±3.2)	12.5 (±0.1)	15.9 (±1.0)	28.9 (±1.4)
	15 d	325.1 (±5.7)	354.7 (±3.6)	47.9 (±3.3)	12.1 (±0.1)	15.5 (±0.7)	30.6 (±0.4)
	30 d	324.1 (±4.3)	352.8 (±3.7)	50.1 (±3.9)	11.3 (±0.1)	13.2 (±0.5)	25.4 (±0.3)
	60 d	313.7 (±5.5)	351.1 (±3.7)	51.5 (±4.1)	10.4 (±0.1)	13.5 (±0.7)	23.6 (±0.3)
	90 d	n.d.*	n.d.*	n.d.*	n.d.*	12.6 (±0.5)	22.5 (±0.3)
Immersion temperature	8 °C	332.0 (±4.7)	356.4 (±2.8)	35.0 (±3.1)	13.4 (±0.1)	24.3 (±0.9)	46.5 (±0.5)
	23 °C	331.1 (±0.5)	356.2 (±2.4)	36.7 (±3.9)	13.4 (±0.1)	22.1 (±1.3)	41.2 (±1.2)
	58 °C	323.1 (±4.4)	354.0 (±3.2)	59.7 (±3.4)	11.3 (±0.1)	7.3 (±0.4)	13.4 (±0.2)
	70 °C	304.9 (±6.4)	347.7 (±5.0)	66.5 (±4.0)	8.3 (±0.1)	2.8 (±0.2)	3.8 (±0.2)
Composition before immersion	PLA	332.4 (±4.2)	355.9 (±1.8)	2.8 (±1.6)	14.3 (±0.0)	39.7 (±0.2)	76.1 (±0.4)
	PLA/PEG	326.3 (±2.6)	356.3 (±1.7)	48.8 (±3.8)	12.9 (±0.1)	23.3 (±0.3)	42.0 (±0.1)
	PLA/PEG/NFC1	327.4 (±2.0)	356.0 (±3.5)	47.1 (±1.5)	13.0 (±0.0)	20.5 (±0.4)	34.3 (±0.1)
	PLA/PEG/NFC3	326.3 (±1.9)	353.8 (±2.7)	42.7 (±1.1)	12.8 (±0.1)	22.3 (±0.1)	35.0 (±0.2)
	PLA/PEG/NFC5	333.2 (±1.2)	356.5 (±0.8)	43.5 (±0.8)	13.1 (±0.0)	24.4 (±0.1)	40.5 (±0.1)
Composition after immersion	PLA	325.7 (±3.6)	354.6 (±2.0)	29.4 (±2.2)	12.3 (±0.1)	22.8 (±1.0)	43.9 (±1.1)
	PLA/PEG	322.7 (±3.6)	355.5 (±2.8)	54.7 (±3.2)	11.5 (±0.1)	13.1 (±0.7)	23.7 (±0.4)
	PLA/PEG/NFC1	324.9 (±5.4)	355.5 (±2.9)	53.8 (±4.1)	11.5 (±0.1)	12.3 (±0.5)	22.4 (±0.4)
	PLA/PEG/NFC3	321.8 (±6.0)	353.2 (±4.2)	54.4 (±4.1)	11.5 (±0.1)	12.4 (±0.7)	21.5 (±0.5)
	PLA/PEG/NFC5	320.4 (±4.3)	349.6 (±4.5)	50.0 (±4.8)	11.6 (±0.1)	13.0 (±0.5)	24.2 (±0.2)

*The samples were vastly disintegrated after 90 days in water at 70 °C, therefore no TGA and DSC analysis could be performed. The missing values made it impossible to calculate the average value for 90 days of immersion time

influences of the other factors are cancelled out. Figure 6 shows the influence of the factors immersion time, temperature, and composition on the values representing the thermo-oxidative stability, crystalline structure and hydrothermal chain scission. For the temperature and composition graphs, the values of the non-immersed samples were added for a better comparison and visualisation of the influence of hydrothermal degradation.

The influence of the immersion time in water on the hydrothermal degradation is represented in the first column of Fig. 6. The thermo-oxidative decomposition temperature and the lamellar thickness, which is directly related to the melting temperature, decreases linearly as a function of time, given the hydrolytic attack on the crystalline domains [7]. In contrast, the degree of crystallinity increases sharply after the first 7 days of immersion and then gradually approaches a plateau. The same
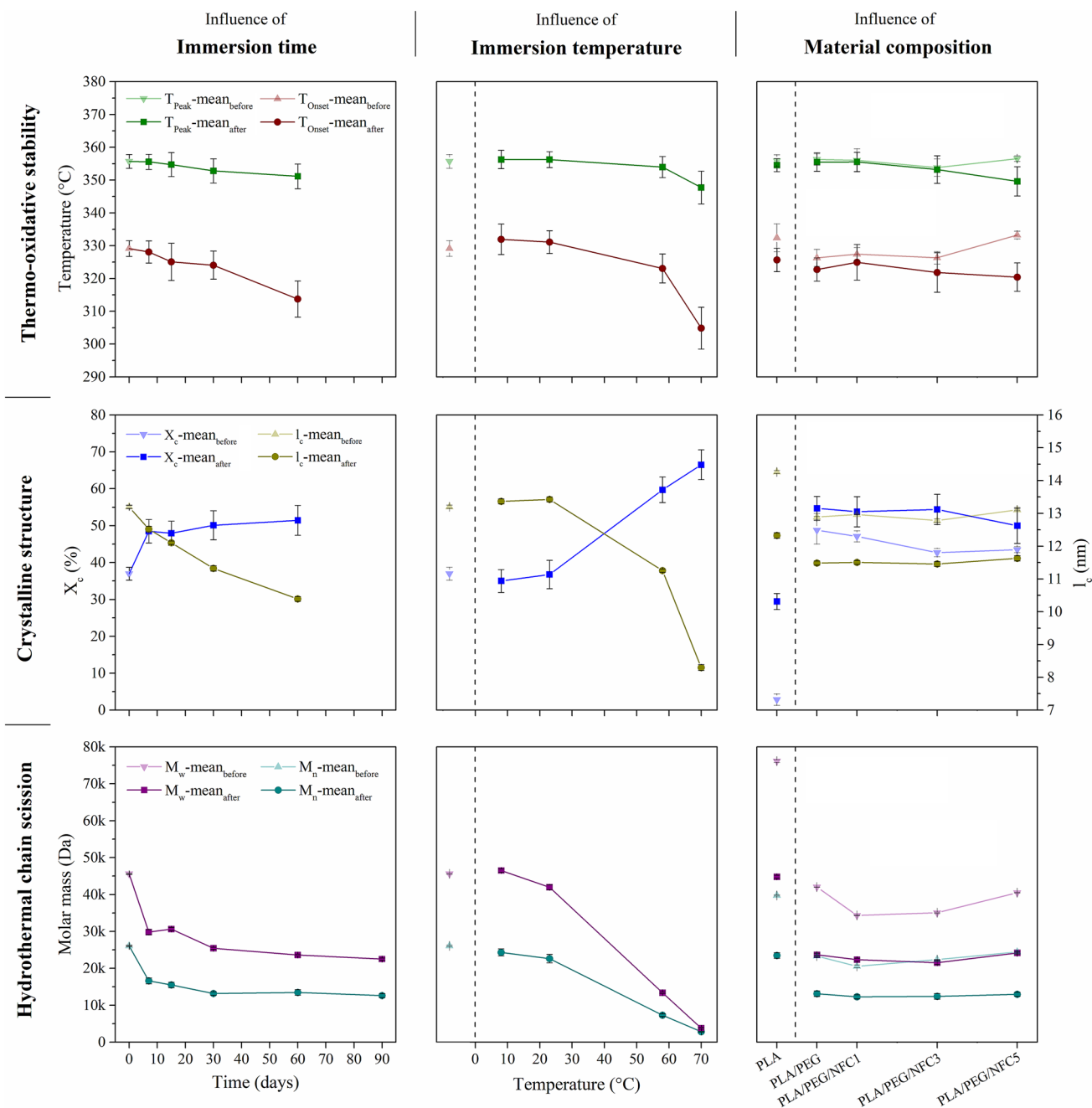
Fig. 6 Influence of the immersion time, temperature, and sample composition on the thermo-oxidative stability (T_{onset}-mean, T_{peak}-mean), the crystalline structure (X_c-mean, l_c-mean), and the hydrothermal chain scission (M_n-mean, M_w-mean)

asymptotic increase in the crystallinity as a function of ageing time was found by Berthe et al. [49] for raw PLA and by Hakkarainen et al. and Gil-Castell et al. for PLA-based materials [7, 71] in their water absorption studies. The profile of the molar mass as a function of immersion time shows a complementary progression to the profile for the degree of crystallinity. The breakage of the PLA chains into smaller segments due to hydrothermal chain scission increases their mobility, allowing them to rearrange into crystalline domains more easily [35]. The asymptotic curve progression indicates a fast-hydrolytic degradation of the amorphous regions in the early stages, followed by a slower degradation of the crystalline regions, which have a higher resilience towards hydrolysis.

The immersion temperature displayed the most significant influence on the hydrothermal degradation of the PLA/PEG/NFC bionanocomposites, as represented in the second column of Fig. 6 [78]. While the physicochemical properties stay almost unaffected through immersion in water at 8 and 23 °C, the values significantly change at 58 °C and even more at 70 °C. For instance, the mean onset temperature of the main decomposition step decreases through the immersion in water at 58 °C around 6 °C and at 70 °C declines up to 24 °C. While the peak temperature seems only slightly affected, the onset temperature decreases considerably, resulting in a greater width of the decomposition step. Furthermore, the degree of crystallinity of the materials increases significantly due to the lower molar mass caused by hydrolytic chain scission, which transforms the amorphous regions into crystalline phases. Other studies also found that the extent of these transformations is increased in environments with higher temperatures [41, 42, 49, 68, 84]. Additionally, it is well known that water can penetrate into the polymer matrix and act as a plasticiser resulting in increased chain mobility and thus creating more crystalline domains, as reported in other water absorption studies [7, 40, 41, 46, 48, 69, 76, 89]. The combination of water and temperature results in an exponential profile for the crystallinity between 8 and 70 °C. The substantial increase in crystallinity of the samples immersed at higher temperatures explains the previous observation of the films becoming white, non-transparent, and fragile after storage in water. The molar mass profile shows a complementary curve progression compared to the degree of crystallinity, showing a strong decrease in the molar mass of PLA/PEG/NFC bionanocomposites at 58 and 70 °C to values down to around 2.5 kDa after 90 days. At such high temperatures, the materials are above their glass transition, which significantly promotes the hydrolysis reaction resulting in severe polymer chain breakage and, thus, highly crystalline structures. This substantial molar mass decrease due to chain breakage at higher temperatures creates smaller oligomers with carboxyl end groups that are more soluble in water and result in the

previously mentioned mass loss, pH reduction and disintegration behaviour of the films.

Finally, the relevance of the composition of the materials on the hydrothermal degradation behaviour was analysed in the third column of Fig. 6. Thermo-oxidative stability given by the onset and peak temperatures of decomposition remained practically unaltered regardless of the NFC addition. In terms of crystalline structure, raw PLA had a lower crystallinity than the PLA/PEG blend and the PLA/PEG/NFC bionanocomposites, both before and after water immersion. However, through the water immersion, the degree of crystallinity for raw PLA increased on average by 26.6% (+ 950%), while the crystallinity for the PLA/PEG blend rose slightly by 5.9% (+ 12%), and the PLA/PEG/NFC nanocomposites increased by 6.5 to 11.7% (+ 14 to + 27%, respectively). This indicates that raw PLA could have a more substantial potential to increase crystallinity during immersion. However, it must be considered that the blend and bionanocomposite materials could be more restrained given that they already had a high degree of crystallinity of ~ 45% before the immersion. In this regard, it is relevant to mention that the NFC percentage of up to 3%wt seemed to enhance crystallisation due to the nucleating performance of the nanoparticles that enhanced crystallinity degree in the non-immersed samples. Greater percentages of NFC may have resulted in nanoparticle agglomeration, which buffered the nucleation ability and resulted in a lower crystalline fraction. This behaviour is aligned with other studies in the literature, all referring to a nucleating effect of the nanofillers up to agglomeration [90–93]. The analysis of the molar mass revealed that raw PLA also had a significantly higher molar mass before the immersion compared to the PLA/PEG blend and the PLA/PEG/NFC bionanocomposites. Nevertheless, when subjected to hydrothermal ageing, all the materials exhibit a comparable decrease in average molar mass of about 40%, regardless of the composition. The higher molar mass of PLA compared to the PLA/PEG blend and the PLA/PEG/NFC bionanocomposites before water immersion explains its lower degree of crystallinity. The chains in the PLA/PEG blend and the PLA/PEG/NFC bionanocomposites were able to move and rearrange themselves more freely during processing due to their shorter length and the plasticising effect of PEG. Dorgan et al. suggest that the entanglement molecular weight of PLA is around 9 kDa [52]. Therefore, the long chains of PLA before immersion may have been highly entangled that movement during processing was hindered, so they were prevented from crystallisation. The processing of the PLA/PEG blend and, in particular, the PLA/PEG/NFC bionanocomposites contributed to the formation of low molar mass compounds, which are then released during immersion, as shown in Fig. 2 from the stronger pH decrease of the solution after immersion in water at 8 °C and 23 °C. Hydrothermal degradation at 58 and

70 °C promoted the breakage of the long chains of raw PLA into smaller segments down to 2.5 kDa. Consequently, the small and hydrolysed segments that are less entangled can rearrange themselves easier, resulting in a more significant increase in the crystallinity of raw PLA and the release of acidic compounds.

Conclusions

From a technological point of view, several insights can be gathered from this study. The hydrothermal degradation behaviour was not critically affected regardless of the nanofibrillated cellulose (NFC) content. This indicates that it could be possible to improve the properties of poly(ethylene glycol) (PEG)-plasticised poly(lactide) (PLA) with NFC as a reinforcement filler without exhibiting more remarkable physicochemical changes in contact with water. The immersion of the PLA/PEG/NFC bionanocomposites in water at temperatures above their glass transition (58 °C and, especially, 70 °C) leads to a drastic decrease in their physicochemical properties, highlighting the limited use in applications in contact with water at these temperatures. However, the observed advanced degradation and disintegration may be feasible for waste management or molecular recycling of these materials by deposition in hot aqueous environments. In contrast, the PLA/PEG/NFC nanocomposites revealed certain integrity towards water immersion and hydrolysis effects after 90 days of immersion in water at lower temperatures (8 °C or 23 °C), indicating a potential use of the materials in water-contact applications at ambient temperatures and limited exposure times, such as in food packaging. Finally, the observed hydrothermal stability at low temperatures indicates that these PLA/PEG/NFC bionanocomposites cannot decompose sufficiently and could lead to waste accumulation if disposed of in cold, humid environments.

Declarations

References

1. Shah S, Matkawala F, Garg S et al (2020) Emerging trend of bio-plastics and its impact on society. Biotechnol J Int 24:1–10. https://doi.org/10.9734/bji/2020/v24i430107

2. Mohanty AK, Misra M, Hinrichsen G (2000) Biofibres, biodegradable polymers and biocomposites: an overview. Macromol Mater Eng 276–277:1–24. https://doi.org/10.1002/(SICI)1439-2054(20000301)276:1%3c1::AID-MAME1%3e3.0.CO;2-W

3. Winkworth-Smith C, Foster TJ (2013) General overview of biopolymers. Structure, properties, and applications. Handbook of biopolymer-based materials. Wiley-VCH, Weinheim, pp 7–36

4. Ray SS, Okamoto M (2003) Biodegradable polylactide and Its nanocomposites: opening a new dimension for plastics and composites. Macromol Rapid Commun 24:815–840

5. Matuana LM (2008) Solid state microcellular foamed poly(lactic acid): morphology and property characterization. Bioresour Technol 99:3643–3650. https://doi.org/10.1016/j.biortech.2007.07.062

6. Verma D, Fortunati E (2019) Biobased and biodegradable plastics. Handb Ecomater 4:2955–2976. https://doi.org/10.1007/978-3-319-68255-6_103

7. Gil-Castell O, Badia JD, Ingles-Mascaros S et al (2018) Polylactide-based self-reinforced composites biodegradation: Individual and combined influence of temperature, water and compost. Polym Degrad Stab 158:40–51. https://doi.org/10.1016/j.polymdegradstab.2018.10.017

8. Zubrowska A, Piorkowska E, Bojda J (2018) Novel tough crystalline blends of polylactide with ethylene glycol derivative of POSS. J Polym Environ 26:145–151. https://doi.org/10.1007/S10924-016-0920-2/TABLES/2

9. Brüster B, Addiego F, Hassouna F et al (2016) Thermo-mechanical degradation of plasticized poly(lactide) after multiple reprocessing to simulate recycling: multi-scale analysis and underlying mechanisms. Polym Degrad Stab 131:132–144. https://doi.org/10.1016/j.polymdegradstab.2016.07.017

10. Ding WD, Chang E, Jahani D, et al (2016) Development Of PLA/Cellulosic fibre composite foams using injection molding:

foaming and mechanical properties. Annual Technical Conference—ANTEC, conference proceedings 83:1783–1787

11. Ghalia MA, Dahman Y (2017) Biodegradable poly(lactic acid)-based scaffolds: synthesis and biomedical applications. J Polym Res 24:74. https://doi.org/10.1007/s10965-017-1227-2

12. Sungsanit K, Kao N, Bhattacharya SN (2012) Properties of linear poly(lactic acid)/polyethylene glycol blends. Polym Eng Sci 52:108–116. https://doi.org/10.1002/pen.22052

13. Pascual-Jose B, Badia JD, Múgica A et al (2021) Analysis of plasticization and reprocessing effects on the segmental cooperativity of polylactide by dielectric thermal spectroscopy. Polymer (Guildf) 223:123701. https://doi.org/10.1016/J.POLYMER.2021.123701

14. Li FJ, Liang JZ, Zhang SD, Zhu B (2015) Tensile properties of polylactide/poly(ethylene glycol) blends. J Polym Environ 23:407–415. https://doi.org/10.1007/S10924-015-0718-7/FIGURES/11

15. Jayanth D, Kumar PS, Nayak GC et al (2018) A review on biodegradable polymeric materials striving towards the attainment of green environment. J Polym Environ 26:838–865. https://doi.org/10.1007/s10924-017-0985-6

16. Mukherjee T, Kao N (2011) PLA based biopolymer reinforced with natural fibre: a review. J Polym Environ 19:714–725. https://doi.org/10.1007/S10924-011-0320-6/FIGURES/12

17. Mazur KE, Borucka A, Kaczor P et al (2022) Mechanical, thermal and microstructural characteristic of 3D printed polylactide composites with natural fibers: wood, bamboo and cork. J Polym Environ 30:2341–2354. https://doi.org/10.1007/S10924-021-02356-3/FIGURES/7

18. Suryanegara L, Nakagaito AN, Yano H (2009) The effect of crystallization of PLA on the thermal and mechanical properties of microfibrillated cellulose-reinforced PLA composites. Compos Sci Technol 69:1187–1192. https://doi.org/10.1016/j.compscitech.2009.02.022

19. Mao J, Tang Y, Zhao R et al (2019) Preparation of nanofibrillated cellulose and application in reinforced PLA/starch nanocomposite film. J Polym Environ 27:728–738. https://doi.org/10.1007/s10924-019-01382-6

20. de Souza AG, Barbosa RFS, Rosa DS (2020) Nanocellulose from industrial and agricultural waste for further use in PLA composites. J Polym Environ 28:1851–1868. https://doi.org/10.1007/S10924-020-01731-W/FIGURES/5

21. Auras R, Harte B, Selke S (2004) An overview of polylactides as packaging materials. Macromol Biosci 4:835–864. https://doi.org/10.1002/mabi.200400043

22. Arrieta MP, López J, Ferrándiz S, Peltzer MA (2013) Characterization of PLA-limonene blends for food packaging applications. Polym Test 32:760–768. https://doi.org/10.1016/j.polymertesting.2013.03.016

23. Arrieta M, Samper M, Aldas M, López J (2017) On the use of PLA-PHB blends for sustainable food packaging applications. Materials 10:1008. https://doi.org/10.3390/ma10091008

24. Gan I, Chow WS (2018) Antimicrobial poly(lactic acid)/cellulose bionanocomposite for food packaging application: a review. Food Packag Shelf Life 17:150–161. https://doi.org/10.1016/j.fpsl.2018.06.012

25. Jabeen N, Majid I, Nayik GA (2015) Bioplastics and food packaging: a review. Cogent Food Agric 1:1117749. https://doi.org/10.1080/23311932.2015.1117749

26. Vasile C, Rapa M, Stefan M et al (2017) New PLA/ZnO:Cu/Ag bionanocomposites for food packaging. Express Polym Lett 11:531–544. https://doi.org/10.3144/expresspolymlett.2017.51

27. Sepúlveda FA, Rivera F, Loyo C et al (2022) Poly (lactic acid)/D-limonene/ZnO bio-nanocomposites with antimicrobial properties. J Appl Polym Sci 139:51542. https://doi.org/10.1002/APP.51542

28. Bano K, Pandey R (2018) New advancements of bioplastics in medical applications. Int J Pharm Sci Res 9:402. https://doi.org/10.13040/IJPSR.0975-8232.9

29. Singhvi MS, Zinjarde SS, Gokhale DV (2019) Polylactic acid: synthesis and biomedical applications. J Appl Microbiol 127:1612–1626. https://doi.org/10.1111/jam.14290

30. Morozov AG, Razborov DA, Egiazaryan TA et al (2020) In Vitro study of degradation behavior, cytotoxicity, and cell adhesion of the atactic polylactic acid for biomedical purposes. J Polym Environ 28:2652–2660. https://doi.org/10.1007/S10924-020-01803-X/FIGURES/8

31. Knoch S, Pelletier F, Larose M et al (2020) Surface modification of PLA nets intended for agricultural applications. Colloids Surf A Physicochem Eng Asp 598:124787. https://doi.org/10.1016/j.colsurfa.2020.124787

32. Rychter P, Lewicka K, Rogacz D (2019) Environmental usefulness of PLA/PEG blends for controlled-release systems of soil-applied herbicides. J Appl Polym Sci 136:47856. https://doi.org/10.1002/app.47856

33. Sevostyanov MA, Kaplan MA, Nasakina EO et al (2020) Development of a biodegradable polymer based on high-molecular-weight polylactide for medicine and agriculture: mechanical properties and biocompatibility. Dokl Chem 490:36–39. https://doi.org/10.1134/S0012500820020044

34. Vink ETH, Rábago KR, Glassner DA et al (2004) The sustainability of Natureworks™ polylactide polymers and Ingeo™ polylactide fibers: an update of the future. Macromol Biosci 4:551–564

35. Vink ETH, Rábago KR, Glassner DA, Gruber PR (2003) Applications of life cycle assessment to NatureWorks™ polylactide (PLA) production. Polym Degrad Stab 80:403–419. https://doi.org/10.1016/S0141-3910(02)00372-5

36. Zhou J, Yu J, Bai D et al (2021) AgNW/stereocomplex-type polylactide biodegradable conducting film and its application in flexible electronics. J Mater Sci: Mater Electron 32:6080–6093. https://doi.org/10.1007/s10854-021-05327-5

37. Arjmandi R, Hassan A, Zakaria Z (2017) Polylactic acid green nanocomposites for automotive applications. In: Jawaid M, Salit MS, Alothman OY (eds) Green energy and technology. Springer International Publishing, Cham, pp 193–208

38. Hu RH, Jang MH, Kim YJ et al (2010) Fully degradable jute fiber reinforced polylactide composites applicable to car interior panel. Adv Mat Res 123–125:1151–1154. https://doi.org/10.4028/www.scientific.net/AMR.123-125.1151

39. Notta-Cuvier D, Odent J, Delille R et al (2014) Tailoring polylactide (PLA) properties for automotive applications: Effect of addition of designed additives on main mechanical properties. Polym Test 36:1–9. https://doi.org/10.1016/j.polymertesting.2014.03.007

40. Badia JD, Santonja-Blasco L, Martínez-Felipe A, Ribes-Greus A (2012) Hygrothermal ageing of reprocessed polylactide. Polym Degrad Stab 97:1881–1890. https://doi.org/10.1016/j.polymdegradstab.2012.06.001

41. Gil-Castell O, Badia JD, Kittikorn T et al (2014) Hydrothermal ageing of polylactide/sisal biocomposites. Studies of water absorption behaviour and physico-chemical performance. Polym Degrad Stab 108:212–222. https://doi.org/10.1016/j.polymdegradstab.2014.06.010

42. Gil-Castell O, Badia JD, Kittikorn T et al (2016) Impact of hydrothermal ageing on the thermal stability, morphology and viscoelastic performance of PLA/sisal biocomposites. Polym Degrad Stab 132:87–96. https://doi.org/10.1016/j.polymdegradstab.2016.03.038

43. Badia JD, Monreal L, Sáenz de Juano-Arbona V et al (2014) Dielectric spectroscopy of reprocessed polylactide. Polym Degrad Stab 107:21–27. https://doi.org/10.1016/j.polymdegradstab.2014.04.023

44. Chassenieux C, Durand D, Jyotishkumar P, Thomas S (2014) Biopolymers state of the art, new challenges, and opportunities. Handbook of biopolymer-based materials. Wiley-VCH, Weinheim, pp 1–6

45. Dhakal HN, Zhang ZY, Richardson MOW (2007) Effect of water absorption on the mechanical properties of hemp fibre reinforced unsaturated polyester composites. Compos Sci Technol 67:1674–1683. https://doi.org/10.1016/j.compscitech.2006.06.019

46. Leu YY, Chow WS (2011) Kinetics of water absorption and thermal properties of poly(lactic acid)/organomontmorillonite/poly(ethylene glycol) nanocomposites. J Vinyl Add Tech 17:40–47. https://doi.org/10.1002/vnl.20259

47. Ozkoc G, Kemaloglu S (2009) Morphology, biodegradability, mechanical, and thermal properties of nanocomposite films based on PLA and plasticized PLA. J Appl Polym Sci 114:2481–2487. https://doi.org/10.1002/app.30772

48. Norazlina H, Hadi AA, Qurni AU et al (2019) Effects of multi-walled carbon nanotubes (MWCNTs) on the degradation behavior of plasticized PLA nanocomposites. Polym Bull 76:1453–1469. https://doi.org/10.1007/s00289-018-2454-3

49. Berthé V, Ferry L, Bénézet JC, Bergeret A (2010) Ageing of different biodegradable polyesters blends mechanical and hygrothermal behavior. Polym Degrad Stab 95:262–269. https://doi.org/10.1016/j.polymdegradstab.2009.11.008

50. (2008) ISO 62:2008. Plastics - Determination of water absorption

51. ASTM International (2018) ASTM D570-98, Standard Test Method for Water Absorption of Plastics

52. Greene JP (2014) Sustainable plastic products. In: Greene JP (ed) Sustainable plastics. John Wiley & Sons Inc, New York, pp 145–186

53. Gil-Castell O, Andres-Puche R, Dominguez E et al (2020) Influence of substrate and temperature on the biodegradation of polyester-based materials: polylactide and poly(3-hydroxybutyrate-co-3-hydroxyhexanoate) as model cases. Polym Degrad Stab 180:109288. https://doi.org/10.1016/j.polymdegradstab.2020.109288

54. ASTM International (2004) ASTM D6400-04, Standard Specification for Compostable Plastics

55. ASTM International (2011) ASTM D5338-11, Standard Test Method for Determining Aerobic Biodegradation of Plastic Materials under Controlled Composting Conditions

56. (2010) DIN EN 13432:2000-12, Packaging Requirements for Packaging Recoverable through Composting and Biodegradation Test Scheme and Evaluation Criteria for the Final Acceptance of Packaging

57. (2018) ISO 14855-2:2018, Determination of the Ultimate Aerobic Biodegradability of plastic materials under Controlled Composting Conditions

58. Rodrigues Filho G, Monteiro DS, da Meireles CS et al (2008) Synthesis and characterization of cellulose acetate produced from recycled newspaper. Carbohydr Polym 73:74–82. https://doi.org/10.1016/j.carbpol.2007.11.010

59. Albornoz-Palma G, Betancourt F, Mendonça RT et al (2020) Relationship between rheological and morphological characteristics of cellulose nanofibrils in dilute dispersions. Carbohydr Polym. https://doi.org/10.1016/j.carbpol.2019.115588

60. Yetiş F, Liu X, Sampson WW, Gong RH (2020) Acetylation of lignin containing microfibrillated cellulose and its reinforcing effect for polylactic acid. Eur Polym J 134:109803. https://doi.org/10.1016/J.EURPOLYMJ.2020.109803

61. Bulota M, Kreitsmann K, Hughes M, Paltakari J (2012) Acetylated microfibrillated cellulose as a toughening agent in poly(lactic acid). J Appl Polym Sci 126:E449–E458. https://doi.org/10.1002/APP.36787

62. ASTM International (2014) ASTM D638-14, Standard Test Method for Tensile Properties of Plastics

63. (2008) EN-ISO 291:2008 Plastics - Standard atmoshperes for conditioning and testing

64. (2014) ISO 11358-1:2014 Plastics - Thermogravimetry (TG) of polymers - Part1: General principles

65. Fischer EW, Sterzel HJ, Wegner G (1973) Investigation of the structure of solution grown crystals of lactide copolymers by means of chemical reactions. Kolloid-Zeitschrift und Zeitschrift für Polymere 251:980–990. https://doi.org/10.1007/BF01498927

66. Lauritzen Jr JI, Hoffman JD (1960) Theory of formation of polymer crystals with folded chains in dilute solution. J Res Natl Bur Stand A Phys Chem 64A:73. https://doi.org/10.6028/JRES.064A.007

67. Vasanthakumari R, Pennings AJ (1983) Crystallization kinetics of poly(l-lactic acid). Polymer (Guildf) 24:175–178. https://doi.org/10.1016/0032-3861(83)90129-5

68. Ndazi BS, Karlsson S (2011) Characterization of hydrolytic degradation of polylactic acid/rice hulls composites in water at different temperatures. Express Polym Lett 5:119–131. https://doi.org/10.3144/expresspolymlett.2011.13

69. Le Duigou A, Davies P, Baley C (2009) Seawater ageing of flax/poly(lactic acid) biocomposites. Polym Degrad Stab 94:1151–1162. https://doi.org/10.1016/j.polymdegradstab.2009.03.025

70. Yew GH, Mohd Yusof AM, Mohd Ishak ZA, Ishiaku US (2005) Water absorption and enzymatic degradation of poly(lactic acid)/rice starch composites. Polym Degrad Stab 90:488–500. https://doi.org/10.1016/j.polymdegradstab.2005.04.006

71. Hakkarainen M, Albertsson A-C, Karlsson S (1996) Weight losses and molecular weight changes correlated with the evolution of hydroxyacids in simulated in vivo degradation of homo- and copolymers of PLA and PGA. Polym Degrad Stab 52:283–291. https://doi.org/10.1016/0141-3910(96)00009-2

72. Grizzi I, Garreau H, Li S, Vert M (1995) Hydrolytic degradation of devices based on poly(dl-lactic acid) size-dependence. Biomaterials 16:305–311. https://doi.org/10.1016/0142-9612(95)93258-F

73. Zhu J, Abeykoon C, Karim N (2021) Investigation into the effects of fillers in polymer processing. Int J Lightweight Mater Manuf 4:370–382. https://doi.org/10.1016/j.ijlmm.2021.04.003

74. Beltrán FR, Arrieta MP, Gaspar G et al (2020) Effect of Iignocellulosic nanoparticles extracted from yerba mate (Ilex paraguariensis) on the structural, thermal, optical and barrier properties of mechanically recycled poly(lactic acid). Polymers (Basel). https://doi.org/10.3390/POLYM12081690

75. Sambha'a EL, Lallam A, Jada A (2010) Effect of hydrothermal polylactic acid degradation on polymer molecular weight and surface properties. J Polym Environ 18:532–538. https://doi.org/10.1007/s10924-010-0251-7

76. Fukushima K, Tabuani D, Dottori M et al (2011) Effect of temperature and nanoparticle type on hydrolytic degradation of poly(lactic acid) nanocomposites. Polym Degrad Stab 96:2120–2129. https://doi.org/10.1016/j.polymdegradstab.2011.09.018

77. Kamau-Devers K, Kortum Z, Miller SA (2019) Hydrothermal aging of bio-based poly(lactic acid) (PLA) wood polymer composites: studies on sorption behavior, morphology, and heat conductance. Constr Build Mater 214:290–302. https://doi.org/10.1016/j.conbuildmat.2019.04.098

78. Atalay SE, Bezci B, Özdemir B et al (2021) Thermal and environmentally induced degradation behaviors of amorphous and semicrystalline PLAs through rheological analysis. J Polym Environ 29:3412–3426. https://doi.org/10.1007/s10924-021-02128-z

79. Ahmad Sawpan M, Islam MR, Beg MDH, Pickering K (2019) Effect of accelerated weathering on physico-mechanical properties of polylactide bio-composites. J Polym Environ 27:942–955. https://doi.org/10.1007/s10924-019-01405-2

80. Göpferich A, Langer R (1993) The influence of microstructure and monomer properties on the erosion mechanism of a class of polyanhydrides. J Polym Sci A Polym Chem 31:2445–2458. https://doi.org/10.1002/pola.1993.080311004

81. Mathiowitz E, Jacob J, Pekarek K, Chickering D (1993) Morphological characterization of bioerodible polymers. 3. characterization of the erosion and intact zones in polyanhydrides using scanning electron microscopy. Macromolecules 26:6756–6765. https://doi.org/10.1021/ma00077a010

82. Risyon NP, Othman SH, Basha RK, Talib RA (2020) Characterization of polylactic acid/halloysite nanotubes bionanocomposite films for food packaging. Food Packag Shelf Life 23:100450. https://doi.org/10.1016/j.fpsl.2019.100450

83. Auras R, Lim L-T, Selke S, Tsuji H (2010) Poly(Lactic Acid): synthesis, structures, properties, processing, and applications. John Wiley & Sons Inc, Hoboken

84. Badia JD, Gil-Castell O, Ribes-Greus A (2017) Long-term properties and end-of-life of polymers from renewable resources. Polym Degrad Stab 137:35–57. https://doi.org/10.1016/j.polymdegradstab.2017.01.002

85. Martin O (2001) Poly(lactic acid): plasticization and properties of biodegradable multiphase systems. Polymer (Guildf) 42:6209–6219. https://doi.org/10.1016/S0032-3861(01)00086-6

86. Yasuniwa M, Tsubakihara S, Sugimoto Y, Nakafuku C (2004) Thermal analysis of the double-melting behavior of poly(L-lactic acid). J Polym Sci B Polym Phys 42:25–32. https://doi.org/10.1002/polb.10674

87. Santonja-Blasco L, Moriana R, Badía JD, Ribes-Greus A (2010) Thermal analysis applied to the characterization of degradation in soil of polylactide: I. Calorimetric and viscoelastic analyses. Polym Degrad Stab 95:2185–2191. https://doi.org/10.1016/j.polymdegradstab.2010.08.005

88. Nijenhuis AJ, Colstee E, Grijpma DW, Pennings AJ (1996) High molecular weight poly(L-lactide) and poly(ethylene oxide) blends: thermal characterization and physical properties. Polymer (Guildf) 37:5849–5857. https://doi.org/10.1016/S0032-3861(96)00455-7

89. Jiang N, Yu T, Li Y et al (2019) Hygrothermal aging and structural damage of a jute/poly (lactic acid) (PLA) composite observed by X-ray tomography. Compos Sci Technol 173:15–23. https://doi.org/10.1016/j.compscitech.2019.01.018

90. Raisipour-Shirazi A, Ahmadi Z, Garmabi H (2018) Polylactic acid nanocomposites toughened with nanofibrillated cellulose: microstructure, thermal, and mechanical properties. Iran Polym J (English Edition) 27:785–794. https://doi.org/10.1007/s13726-018-0651-4

91. Almasi H, Ghanbarzadeh B, Dehghannya J et al (2015) Novel nanocomposites based on fatty acid modified cellulose nanofibers/poly(lactic acid): morphological and physical properties. Food Packag Shelf Life 5:21–31. https://doi.org/10.1016/j.fpsl.2015.04.003

92. Fujisawa S, Saito T, Kimura S et al (2013) Surface engineering of ultrafine cellulose nanofibrils toward polymer nanocomposite materials. Biomacromol 14:1541–1546. https://doi.org/10.1021/bm400178m

93. Perić M, Putz R, Paulik C (2019) Influence of nanofibrillated cellulose on the mechanical and thermal properties of poly(lactic acid). Eur Polym J 114:426–433. https://doi.org/10.1016/j.eurpolymj.2019.03.014